VDMA
Fluid Power Association

23rd ISC

International Sealing Conference

Stuttgart, Germany
Sept.30 - Oct.1, 2026

Sealing the future –
Facing the challenges of tomorrow

UNI STUTTGART

Fachverband Fluidtechnik im VDMA e. V. Lyoner Str. 18
50628 Frankfurt am Main
Germany

Phone +49 69 6603-1513
E-Mail maximilian.baxmann@vdma.eu

Internet www.vdma.eu/fluid

Introducing Output-Splitting Physics-Informed Neural Networks: A Novel Method for Guaranteed Regime Selection in Seal Modeling

Georg Michael Puntigam, Darren Lam Ming Hui, Faras Brumand-Poor, Katharina Schmitz

Seals are critical machine elements in pneumatic and hydraulic systems, strongly affecting efficiency, durability, and reliability. However, simulation-based seal design remains computationally expensive due to the strong coupling of nonlinear phenomena, including hydrodynamic pressure, contact mechanics, and lubricant starvation. Elastohydrodynamic (EHD) simulations in particular limit the feasibility of iterative design processes. Recent work has shown that Physics-Informed Neural Networks (PINNs) can efficiently approximate the hydrodynamic component of EHD simulations while preserving physical consistency [1]. A key limitation, however, is the accurate capture of regime transitions between pressurized and starved lubrication states, which are mutually exclusive yet not reliably enforced in conventional PINN architectures. This work introduces a redesigned hydrodynamic PINN (HD-PINN) output structure that explicitly enforces this mutual exclusivity, ensuring physically consistent predictions across the entire domain. The proposed model is validated against a previously published HD-PINN approach [1] and demonstrates robust representation of regime transitions. These results highlight the strong potential of advanced HD-PINN architectures for efficient, reliable seal modeling, enabling faster, more robust simulation-based design of sealing systems. Furthermore, this work showcases limitations that arise from the exclusive usage of the L^2-norm for PINN training.

1 Introduction

The performance, durability, and efficiency of mechanical systems are strongly influenced by the behavior of their tribological interfaces, particularly those involving lubrication, such as seals [2]. Failures in these components can result in downtime, costly maintenance, or even severe system damage. Elastomeric seals are widely used for their simple design and low cost; however, their replacement is often labor-intensive, thereby increasing maintenance effort.

In fluid power applications, seals are essential for maintaining system pressure [3]. Dynamic seals, however, generate friction during operation, which can reduce efficiency and affect performance. This is especially critical in valves, where even small frictional forces can disrupt flow and affect downstream components. Despite their widespread use, particularly in pneumatic systems, the underlying friction mechanisms at these sealing interfaces remain poorly understood [4].

Figure 1 illustrates a pneumatic spool valve consisting of a movable spool within a housing containing multiple ports. The spool is actuated by either a solenoid or pneumatic pressure, and its position determines whether these ports are connected or isolated. Two types of seals are mounted on the spool to prevent leakage. Inner seals (1) engage or disengage with the housing depending on spool position, controlling airflow during switching. Outer seals (2) remain in constant contact to retain pressurized air. The sliding motion between seals and their contact surfaces produces friction.

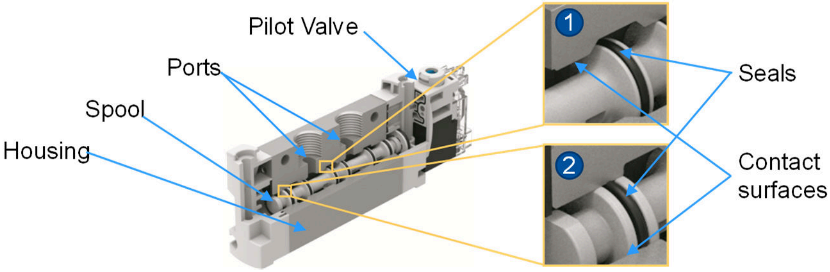

Figure 1: An image of a pneumatic spool valve with its seals. Picture provided by courtesy of Festo. [5]

The hydrodynamic behavior of tribological contacts in such systems is a critical factor in dynamic friction, making accurate modeling indispensable [3]. While simplified analytical models provide initial insights, they often lack precision, whereas experimental studies are time- and resource-intensive. Elastohydrodynamic lubrication (EHL) simulations offer a robust alternative, employing the Reynolds equation, shown in Equation (1), to describe pressure distribution and a material and contact model for the deformation [6].

$$\frac{v}{2}\frac{\partial}{\partial x}\left((1-\theta)\rho h R_q \Phi^{\tau}\right) - \frac{1}{12\eta}\frac{\partial}{\partial x}\left(\Phi^{p}\rho h^{3}\frac{\partial p}{\partial x}\right) + \frac{\partial}{\partial t}\left((1-\theta)\rho h\right) = 0 \tag{1}$$

The classical Reynolds equation by Osborne Reynolds [7] is typically extended to account for surface roughness by the flow factors Φ^{τ} and Φ^{p} derived by Patir and Cheng in Equation (1) [8], [9]. Furthermore, cavitation or starved lubrication film height is modeled by integrating the cavity fraction θ. In the case of a pneumatic valve, the cavity fraction, here denoted as θ is used to model the starved lubrication height in the investigated gap, thus the symbol θ represents how much the gap is starved of lubricant instead of classical cavitation. Note that the all results presented in this paper are applicable for modeling of hydraulic problems with PINNs as well. To obtain a feasible solution an accurate cavitation model is required. In most research, the Jakobsson-Floberg-Olsson (JFO) model [10], [11] is used. The Fischer-Burmeister equation (2) is used to represent the exclusivity of pressure and starved lubrication mathematically.

$$p + \theta - \sqrt{p^2 + \theta^2} = 0 \tag{2}$$

Detailed analysis and optimization of tribological systems typically require significant computational effort to model seal dynamics accurately. To overcome these challenges, various numerical methods are applied [2], [6], [12]. Fluid–structure interaction (FSI) techniques combine finite element analysis (FEA) of structural deformation with the hydrodynamic response of the lubricant [6], [13]. Model Order Reduction (MOR) methods further improve efficiency by projecting the system onto a reduced-dimensional space [14]. Additionally, analytical solutions have been proposed for specific EHL cases [15], [16].

At the Institute of Fluid Power Drives and Systems (ifas) at the RWTH Aachen University, friction in pneumatic valves has been studied using a monolithic EHL simulation framework, Dynamic Description of Sealings (DDS) [17]–[20]. This model integrates hydrodynamic effects with seal deformation and contact mechanics, providing highly accurate results for defined operating conditions. However, its substantial computational requirements limit its suitability for real-time applications.

Brumand et al. have successfully implemented Physics-Informed Neural Networks (PINNs) for the accelerated computation of the hydrodynamic [1], [19] and deformation [21], [22] part of the DDS. Several other researchers have also worked on solving different variants of the Reynolds equation with hydrodynamic PINNs (HD-PINNs). To the knowledge of the authors, all researchers have chosen to implement two outputs to model pressure and cavitation/starvation as listed in Table 1.

Table 1: Summary of neural network architecture by different authors.

Author	Inputs	Layers	Layer Size	Output
Almqvist [23]	x	1	10	p
Cheng et al. [24]	x, y	6	20	p
Hess et al. [25]	$h_{x,y}$	6	Three-dim, see paper	p
Ramos et al. [26]	x, y, ϵ, α $x, y, \epsilon, \alpha, u, v$	7 6	(4,12,50,50,25,12,1) (6, 15, 60, 60,15,1)	p
Rimon et al. [27]	x	4	30	p, Q
Rom [28]	x, y x, y, e_{rel}	6 6	20 20	p, θ
Xi et al. [29]	x	3	64	p, θ
Zhao et al. [30]	x, y	2,3 and 4	16, 32	p

The challenge in this design is the necessity for solving the Fischer-Burmeister equation to obtain exclusivity between pressure and cavitation/starvation. The transition regime remains a challenge, since PINNs with the conventional output design often struggle to separate pressure and cavitation/starvation regions properly. Brumand et al., for example, had to introduce a soft-constraint loss to obtain HD-PINN predictions of good quality [1]. In this work, a redesigned HD-PINN output is presented to improve regime transition modeling. The redesign significantly reduces the number of loss terms. In addition, the PINN framework is extended to enforce boundary conditions (BCs), further reducing the number of required loss terms and resulting in faster training and better performance. The novel redesign is compared to the PINN of Brumand et al., which was presented in prior work at the 22nd International Sealing Conference in Stuttgart [1]. This PINN will also be referred to as “Legacy PINN”. The next Section introduces the redesigned output. Section 3 presents the investigated test case and the underlying variant of the Reynolds Equation. Section 4 yields the results of the legacy framework and the redesigned framework and eventually, a discussion and an outlook are provided.

2 Output redesign for guaranteed exclusive Pressure and Lubrication Starvation Regimes

To obtain a clear separation between pressure and lubrication starvation regimes, a HD-PINN design with one output u_1 for both pressure and lubrication starvation is possible, a second output u_2 is needed only for gradient sharpness. The range of physically meaningful pressure values p are positive real numbers. The physically meaningful range of the starved film height fraction θ is zero to one. Exemplary values are shown in Figure 2.

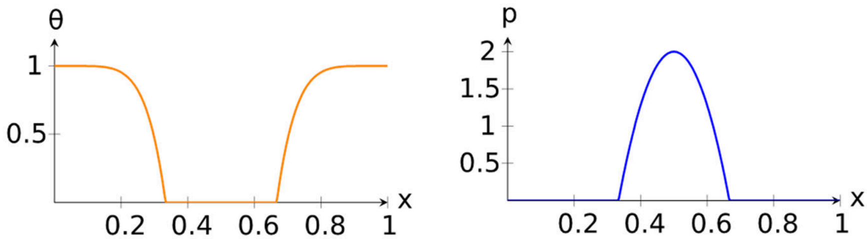

Figure 2: Isolated pressure and starved film height outputs

Therefore, values of a single output u_1 can be split at 0 into p and θ as shown in Equations (3) and (4), where output u_2 is multiplied with the starved film height value.

$$\begin{aligned} \hat{p} &= u_1, && u_1 > 0 \\ \hat{p} &= 0, && u_1 \leq 0 \end{aligned} \tag{3}$$

$$\begin{aligned} \hat{\theta} &= -u_1 \cdot (1 + u_2), && u_1 \leq 0 \\ \hat{\theta} &= 0, && u_1 > 0 \end{aligned} \tag{4}$$

Figure 3 shows the combined output u_1 of the redesigned PINN. The second output u_2 is limited to positive real values and not shown. The gradient sharpness is needed to improve modelling of discontinuities in the pressure-cavitation curve that can arise during regime transitions. While a single output theoretically should be sufficient, in practise a second output for sharpness seems to be necessary.

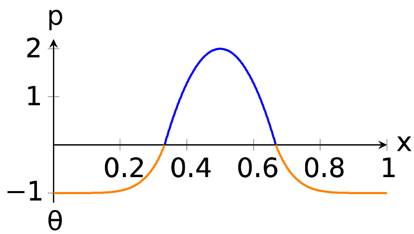

Figure 3: Combined output

With the new output design concept, the Fischer-Burmeister Equation (1) is automatically fulfilled and does not need to be optimized. Soft-Constraint losses are no longer required. Additionally, in the previous output design, pressure and starvation boundary conditions on the right side of the domain required two separate losses during the optimization process; with the new design, one loss is sufficient. Only one boundary condition can have a positive value; the other one is zero. Whenever the non-zero boundary condition is satisfied, the other is satisfied by the redesign.

Regarding the implementation, a challenge arises in computing the gradients for the optimizer. The optimization problem for a Neural Network is briefly described below. The goal is to determine the optimal parameter set Θ^* of weights W^k and biases b^k for all network layers n_D such that the network output $\hat{y}(x;\Theta)$ approximates the desired target output y for a given input x.

$$\Theta^* = \{W^k, b^k\}_{k=1}^{n_D} \tag{5}$$

$$J(\theta^*) = \mathcal{L}(\hat{y}(x;\Theta), y) \tag{6}$$

Loss functions are denoted as $\mathcal{L}$. The proposed output split in Equations (3) and (4) prevents the chosen optimizer from observing meaningful descent directions for pressure values in areas of lubrication starvation and vice versa for the Reynolds equation during backpropagation. The value of the Reynolds loss depends on the PINN's predictions for pressure $\hat{p}$ and lubrication starvation $\hat{\theta}$, which themselves depend on input values x and the current network parameters Θ. This means that without further measure, pressure and lubrication starvation regimes would be optimized separately. The optimizer would not receive information on how to change network parameters in order to change pressure values into starved film height values and vice versa. Mathematically this is shown in Equations (7) and (8).

$$\frac{\delta}{\delta\Theta}\mathcal{L}_{Reynolds}\big(\hat{p}(x;\Theta)\big) = 0 \quad | \, u_1 \leq 0 \tag{7}$$

$$\frac{\delta}{\delta\Theta}\mathcal{L}_{Reynolds}\left(\hat{\theta}(x;\Theta)\right) = 0 \quad | \, u_1 > 0 \tag{8}$$

For every point in the simulation domain, the optimizer could only improve pressure and lubrication starvation magnitudes, but not whether that point should have pressure or starved film height in general. To address this issue, a straight-through estimator (STE) is employed, using a scaled Softplus function $\frac{1}{\beta}\ln(1+e^{\beta x})$ to provide gradients for the optimizer:

$$p_{STE} = \frac{1}{\beta}\ln(1+e^{\beta u_1}) \tag{11}$$

$$\theta_{STE} = \frac{1}{\beta}\ln(1+e^{\beta(-u_1)(1+u_2)}) \tag{12}$$

The losses are still computed from pressure and lubrication starvation values $\hat{p}$ and $\hat{\theta}$ but the optimizer observes the values from the STE, $\hat{p}_{STE}$ and $\hat{\theta}_{STE}$, where loss gradients with respect to network parameters are generally non-zero:

$$\frac{\delta}{\delta\Theta}\mathcal{L}_{Reynolds}\left(\hat{p}_{STE}(x;\Theta)\right) \neq 0 \tag{13}$$

$$\frac{\delta}{\delta\Theta}\mathcal{L}_{Reynolds}\left(\hat{\theta}_{STE}(x;\Theta)\right) \neq 0 \tag{14}$$

With the STE, the PINN can learn pressure and lubrication starvation magnitudes for every point in the simulation domain as well as whether pressure or lubrication starvation should appear at that point.

3 Investigation of improved model performance

The performance of the redesign is compared to the same test case from the previous framework [1]. A stationary case with starved film height is investigated. With $\rho = 1, R_q = 1, \Phi^{\tau} = 1, \Phi^{p} = 0, \frac{\partial\cdot}{\partial t} = 0,$ the Reynolds Equation (1) is simplified to the equation below:

$$\frac{\partial}{\partial x}\left((1-\theta)h\right) - \frac{1}{12\eta}\frac{\partial}{\partial x}\left(h^3\frac{\partial p}{\partial x}\right) = 0 \tag{15}$$

3.1 Stationary Starved Film Height

Table 2 summarizes the test case previously introduced in [1] for simulating a stationary starved film height scenario. The setup consists of a diverging gap and a horizontal relative motion of the housing against the counter surface. This configuration captures characteristic features of starved film height, especially the steep gradient at the interface between starvation and pressure regions. As such, it serves as an excellent benchmark for assessing the redesign.

Table 2: Investigated test scenario.

Scenario	Domain	$\frac{\partial ..}{\partial t}$	v	Boundary Conditions	Gap Geometry
Stationary Starved Film Height	$x = [0,1]$ $n_x = 200$ $t = 0$ $n_x = 1$	$\frac{\partial \theta}{\partial t} = 0$ $\frac{\partial h}{\partial t} = 0$	1	$p_{left} = 0.7$ $p_{right} = 0.2$ $\theta_{left} = 0$ $\theta_{right} = 0$	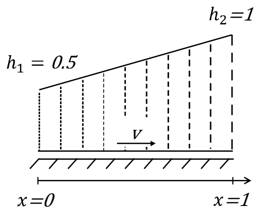

3.2 HD-PINN architecture of the legacy and new framework

In Figure 4 the HD-PINN architecture of the legacy framework is displayed. The PINN has two outputs and the Fischer-Burmeister loss to account for starvation. Automatic differentiation (AD) is performed to obtain gradients of network outputs with respect to inputs. In figures Figure 4 and Figure 5, I denotes the identity function, indicating that unchanged output values also are passed on to the calculation of losses.

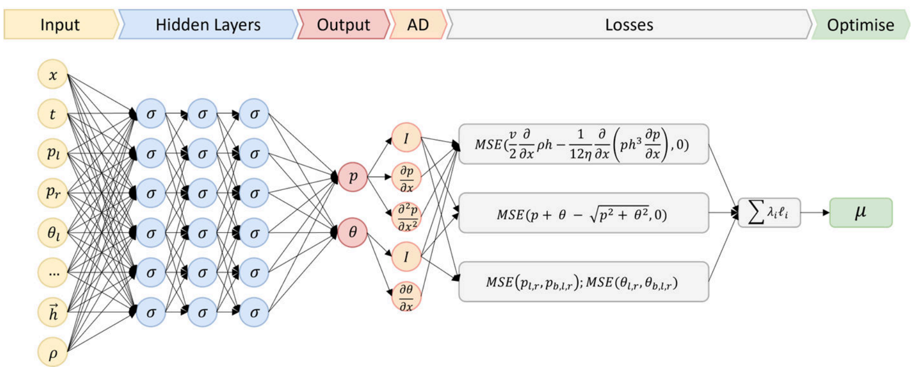

Figure 4: HD-PINN architecture of the legacy framework

In comparison to the legacy framework, Figure 5 shows the redesigned output. The number of losses is reduced to two. Also, notice the STE illustration, passing over u_1 and u_2 during backpropagation.

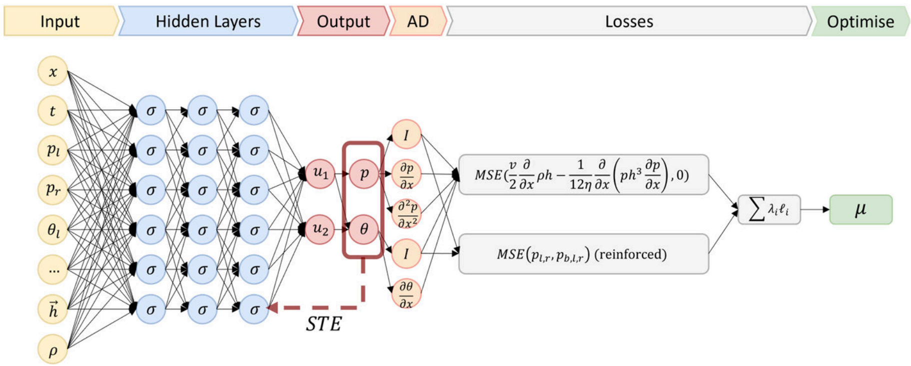

Figure 5: HD-PINN architecture of this work's framework

4 Results

In the following chapter, the results are presented. Starting with the legacy framework, Figure 6 illustrates the pressure distribution and starved film height in the investigated gap. On the right side, the actual lubrication height is illustrated.

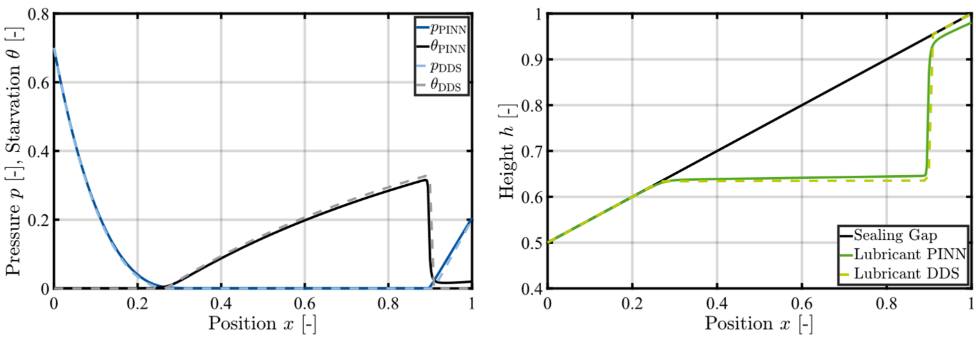

Figure 6: Pressure distribution and starvation for the stationary scenario and the lubrication height from legacy framework

The results shown are no different from those provided in the previous results [1]. The PINN can solve the test case accurately, however, the region $x > 0.9$ does contain non-zero values for both parameters. The Fischer-Burmeister equation is suboptimally preserved here. A problem that the redesign framework aims to tackle. Figure 7 shows the novel framework, with enforced boundaries.

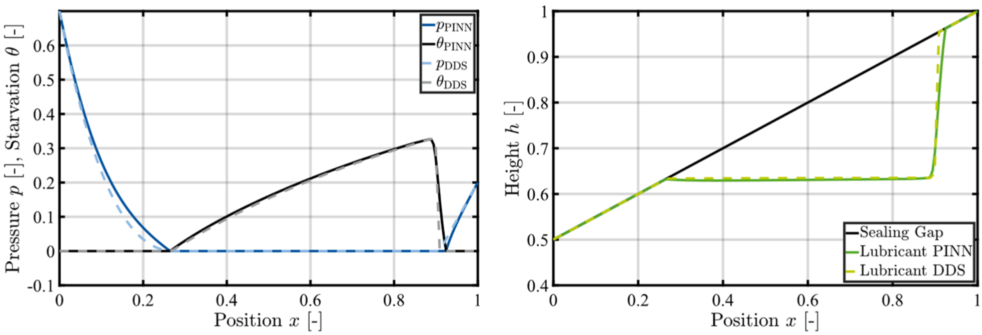

Figure 7: Pressure distribution and starved lubrication for the stationary scenario and the lubrication height from the redesigned framework with enforced boundary conditions.

Based on the pressure and starved film height distributions, the transitions between pressure and starved film height are much more sharply defined than in the legacy framework. However, the general distribution of pressure and starved film height shows greater deviation from the DDS results as compared to the legacy framework.

The last presented result is shown in Figure 8 for the novel framework, without enforced boundary conditions. The results resemble the prior distribution. Overall, the PINN can capture the underlying physics and switches between both regions, however the overall derivation is higher compared to the legacy framework. In both cases of the novel framework, the position of the transition is not equal to the one computed by the iterative solver.

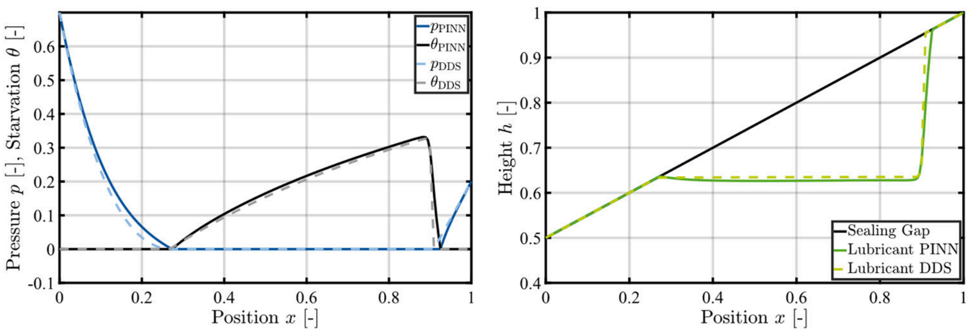

Figure 8: Pressure distribution and starvation for the stationary scenario and the lubrication height from the redesigned framework without enforced boundary conditions

5 Discussion

To obtain a better understanding of the new features, Figure 9 is presented. The plot compares the summed losses across the different frameworks, with all curves smoothed using a moving-average filter with a window size of 5000. The new framework reaches lower loss magnitudes much faster than the legacy framework and maintains lower magnitudes across almost the entire training period. The new framework without reinforced boundary conditions reaches the lowest total loss at the end of training. Reinforced boundary conditions initially accelerate the training substantially but fall behind the training without reinforced boundary conditions after some time.

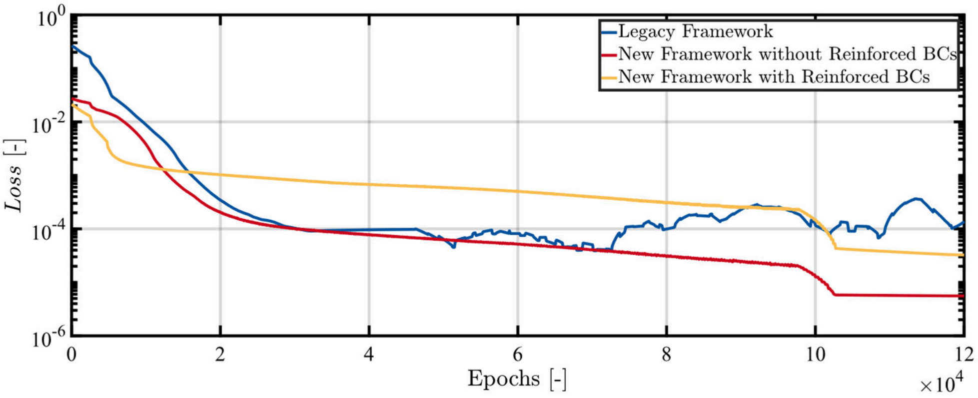

Figure 9: Comparison of summed loss progress over the training duration.

The reduced number of objective terms in the new framework enables the HD-PINN to optimize the loss more efficiently. By contrast, the legacy framework requires some form of loss balancing to reduce conflicts between the individual loss terms during training which also increases the runtime of the training. This can also be observed in its loss trajectory, which exhibits more frequent spikes and oscillations throughout training. Such behaviour suggests competing optimization targets among the different loss components, resulting in less stable convergence behaviour.

Regarding the deviation from the DDS solutions in Figures Figure 7 and Figure 8, the reason is the use of a global L^2-norm residual, which averages the error over the entire domain. Therefore, spikes in local error which occur at transitions from pressure to starved film height and vice versa can be tolerated and eventually neglected. The problem is shown in Figure 10. Even though the new framework achieves a lower a global L^2-norm, the loss spikes that can be observed around the regime transitions lead to more deviation from the DDS solution compared to the Legacy Framework solution.

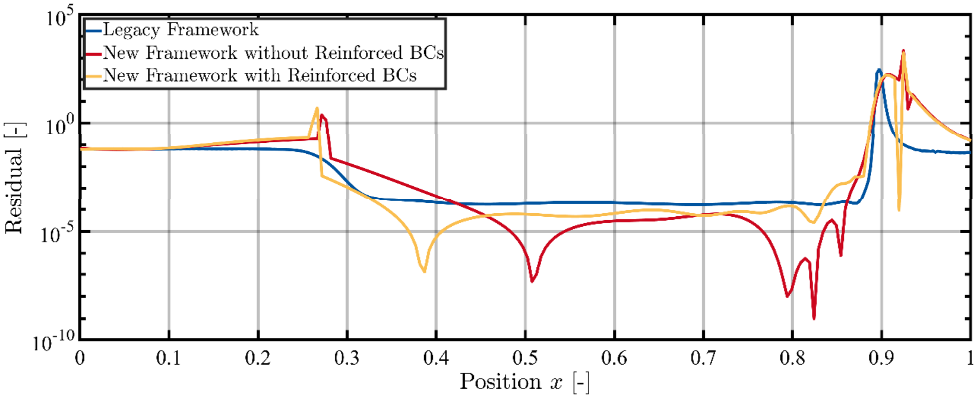

Figure 10: Comparison of residual of each framework over the spatial domain.

6 Summary and Conclusion

This paper presented a redesigned HD-PINN output formulation for EHD seal simulation, with a guaranteed separation between pressure and lubrication starvation regimes. By embedding the regime separation directly into the network output, the proposed approach eliminates the need for optimizing the Fischer-Burmeister equation and removes auxiliary soft-constraint losses, thereby reducing the number of objective terms in training.

The redesign was assessed using the stationary starved film height test case from the previous framework. The results showed that the new formulation yields a much sharper and more physically consistent transition between pressure and starved film height regions than the legacy framework. In addition, the framework without reinforced boundary conditions achieved the lowest total loss and generally converged faster. This demonstrates that the HD-PINN can focus more effectively on residual optimization while avoiding the loss-balancing difficulties observed in the legacy approach. However, the results also indicate that further improvement is needed in the overall agreement with the DDS reference solution. In particular, the use of a global L^2-norm residual may smooth out local errors and limit accuracy in regions with steep gradients. Future work should therefore investigate alternative residual norms and extend the redesigned framework to transient starved film height test cases.

7 Acknowledgements

The authors thank the Research Association for Fluid Power of the German Engineering Federation VDMA for its financial support. Special gratitude is expressed to the participating companies and their representatives in the accompanying industrial committee for their advisory and technical support.

8 Nomenclature

Variable	*Description*	*Unit*
h	Gap height	[-]
h_{lub}	Lubrication height	[-]
h_1	Height at the left end	[-]
h_2	Height at the right end	[-]
h_3	Curvature of sealing	[-]
h_4	Position for sealing bend	[-]
n_t	Time collocation points	[-]
n_x	Position collocation points	[-]
p	Hydrodynamic pressure	[-]
$p_{b,l,r}$	Pressure boundary condition for left and right boundary	[-]
$p_{l,r}$	Pressure at the left and right boundary	[-]
θ	Cavity friction	[-]
$\theta_{b,l,r}$	Pressure boundary condition for left and right boundary	[-]
$\theta_{l,r}$	Pressure at the left and right boundary	[-]
p_{STE}	Pressure Straight-Through-Estimator function	[-]
θ_{STE}	Cavitation Straight-Through-Estimator function	[-]
t	Time	[-]
v	Velocity of the counter surface	[-]
x	Axial coordinate	[-]
η	Fluid viscosity	[-]
$\frac{\partial ..}{\partial x,t}$	Partial differentiation regarding time and position	[-]
σ	Single artificial neuron	[-]
W^k	Weight in artificial neuron k	[-]
b^k	Bias in artificial neuron k	[-]
$\mathcal{L}$	Loss Function	[-]
Φ^p	Pressure flow factors	[-]
Φ^τ	Shear flow factors	[-]
R_q	Root mean squared contact surface roughness	[-]

9 Authors

RWTH Aachen University, Institute for Fluid Power Drives and Systems (ifas) Campus-Boulevard 30, 52074 Aachen, Germany:

Georg Michael Puntigam M.Sc., ORCID 0009-0009-9472-6323, georg.puntigam@ifas.rwth-aachen.de

Darren Lam Ming Hui B.Sc., ORCID 0009-0003-6617-568X, darren.lam@ifas.rwth-aachen.de

Faras Brumand-Poor M. Sc., M. Sc., ORCID 0009-0006-7442-8706, faras.brumand@ifas.rwth-aachen.de

Univ.-Prof. Dr.-Ing. Katharina Schmitz, ORCID 0000-0002-1454-8267, katharina.schmitz@ifas.rwth-aachen.de

10 References

[1] F. Brumand-Poor, F. Barlog, N. Plückhahn, M. Thebelt, and K. Schmitz, *Advancing Lubrication Calculation: A Physics-Informed Neural Network Framework for Transient Effects and Cavitation Phenomena in Reciprocating Seals*. Stuttgart, Germany.

[2] A. Wohlers, O. Heipl, B. N. J. Persson, M. Scaraggi, and H. Murrenhoff, "Numerical and Experimental Investigation on O-Ring-Seals in Dynamic Applications," *International Journal of Fluid Power*, vol. 10, no. 3, pp. 51–59, 2009, doi: 10.1080/14399776.2009.10780988.

[3] J. B. Angerhausen, H. Murrenhoff, B. N. J. Persson, and K. Schmitz, "Physically Motivated Simulation of Dynamic Hydraulic Seals," in *Proceedings of the ASME/BATH Symposium on Fluid Power and Motion Control - 2019*, 2020, V001T01A013. [Online]. Available: https://publications.rwth-aachen.de/record/783017

[4] K. Schmitz and H. Murrenhoff, *Grundlagen der Fluidtechnik: Teil 1: Hydraulik,* 9th ed. Aachen: Shaker Verlag, 2018. [Online]. Available: https://www.shaker.de/shop/978-3-8440-6246-5

[5] Festo SE & Co. KG. 2018, *Valve and valve terminal series VG [online].* [Online]. Available: https://media.festo.com/media/2988_documentation.pdf (accessed: Mar. 14 2025).

[6] N. Dakov, "Elastohydrodynamische Simulation von Wellendichtungen am Beispiel der PTFE-Manschettendichtung mit Rückförderstrukturen," 2020.

[7] O. Reynolds, "On the Theory of Lubrication and Its Application to Mr. Beauchamp Tower's Experiments, Including an Experimental Determination of the Viscosity of Olive Oil," *Philosophical Transactions of the Royal Society of London*, vol. 177, pp. 157–234, 1886.

[8] N. Patir and H. S. Cheng, "An Average Flow Model for Determining Effects of Three-Dimensional Roughness on Partial Hydrodynamic Lubrication," *Journal*

of Lubrication Technology, vol. 100, no. 1, pp. 12–17, 1978, doi: 10.1115/1.3453103.

[9] N. Patir and H. S. Cheng, "Application of Average Flow Model to Lubrication Between Rough Sliding Surfaces," *Journal of Lubrication Technology*, vol. 101, no. 2, pp. 220–229, 1979, doi: 10.1115/1.3453329.

[10] "The finite journal bearing, considering vaporization," *Wear*, vol. 2, no. 2, p. 158, 1958, doi: 10.1016/0043-1648(58)90453-8.

[11] K. O. Olsson, "Cavitation in Dynamically Loaded Bearings," Chalmers University of Technology, Gothenburg Technical Report No. 308, 1965.

[12] Ping Huang, *Numerical Calculation of Elastohydrodynamic Lubrication: Methods and Programs*: Wiley, 2015. [Online]. Available: https://www.wiley.com/en-us/Numerical+Calculation+of+Elastohydrodynamic+Lubrication%3A+Methods+and+Programs-p-9781118920992

[13] W. Habchi, S. Bair, and P. Vergne, "On friction regimes in quantitative elastohydrodynamics," *Tribology International*, vol. 58, pp. 107–117, 2013, doi: 10.1016/j.triboint.2012.10.005.

[14] D. Maier, "On the Use of Model Order Reduction Techniques for the Elastohydrodynamic Contact Problem," 2015.

[15] J. Echávarri Otero, E. de La Guerra Ochoa, E. Chacón Tanarro, F. Franco Martínez, and R. W. Contreras Urgiles, "An Analytical Approach for Predicting EHL Friction: Usefulness and Limitations," *Lubricants*, vol. 10, no. 7, p. 141, 2022, doi: 10.3390/lubricants10070141.

[16] M. Simpson, R. Rahmani, N. Dolatabadi, N. Morris, D. Jones, and C. Craig, "An analytical friction model for point contacts subject to boundary and mixed elastohydrodynamic lubrication," *Tribology International*, vol. 196, p. 109699, 2024, doi: 10.1016/j.triboint.2024.109699.

[17] N. Bauer, "Elastohydrodynamik pneumatischer Dichtsysteme," Dissertation, RWTH Aachen University, Düren, 2025. [Online]. Available: https://publications.rwth-aachen.de/record/1003655

[18] F. Brumand-Poor, N. Bauer, N. Plückhahn, and K. Schmitz, *Fast Computation of Lubricated Contacts: A Physics-Informed Deep Learning Approach*. Dresden, Germany.

[19] F. Brumand-Poor, F. K. Azanledji, N. Plückhahn, F. Barlog, L. Boden, and K. Schmitz, "Extrapolation of cavitation and hydrodynamic pressure in lubricated contacts: a physics-informed neural network approach," *Adv. Model. and Simul. in Eng. Sci.*, vol. 12, no. 1, 2025, doi: 10.1186/s40323-025-00283-9.

[20] J. B. Angerhausen, "Physikalisch motivierte, transiente Modellierung translatorischer Hydraulikdichtungen," Dissertation, RWTH Aachen University, Düren, 2020. [Online]. Available: https://publications.rwth-aachen.de/record/803226

[21] F. Brumand-Poor, N. Plückhahn, and K. Schmitz, *Accelerating Computation of Sealing Deformation - A Physics-Informed Neural Network Framework for Hyperelastic Deformation*.

[22] F. Brumand-Poor, M. Trautmann, and K. Schmitz, "Advancing deformation calculation: a physics-informed deep graph learning framework for hyperelastic materials," *Adv. Model. and Simul. in Eng. Sci.*, vol. 12, no. 1, 2025, doi: 10.1186/s40323-025-00304-7.
[23] A. Almqvist, "Fundamentals of Physics-Informed Neural Networks Applied to Solve the Reynolds Boundary Value Problem," *Lubricants*, vol. 9, no. 8, p. 82, 2021, doi: 10.3390/lubricants9080082.
[24] Y. Cheng, Q. He, W. Huang, Y. Liu, Y. Li, and D. Li, "HL-nets: Physics-informed neural networks for hydrodynamic lubrication with cavitation," *Tribology International*, vol. 188, p. 108871, 2023, doi: 10.1016/j.triboint.2023.108871.
[25] N. Hess and L. Shang, "Development of a Machine Learning Model for Elastohydrodynamic Pressure Prediction in Journal Bearings," *Journal of Tribology*, vol. 144, no. 8, 2022, doi: 10.1115/1.4053815.
[26] D. J. Ramos, B. Z. Cunha, and G. B. Daniel, "Evaluation of physics-informed neural networks (PINN) in the solution of the Reynolds equation," *Journal of the Brazilian Society of Mechanical Sciences and Engineering*, vol. 45, no. 11, 2023, doi: 10.1007/s40430-023-04418-0.
[27] M. T. I. Rimon, M. F. Hassan, K. R. Lyathakula, S. Cesmeci, H. Xu, and J. Tang, Eds., *A Design Study of an Elasto-Hydrodynamic Seal for sCO2 Power Cycle by Using Physics Informed Neural Network*, 2023.
[28] M. Rom, "Physics-informed neural networks for the Reynolds equation with cavitation modeling," *Tribology International*, vol. 179, p. 108141, 2023, doi: 10.1016/j.triboint.2022.108141.
[29] Y. Xi, J. Deng, and Y. Li, "A new method to solve the Reynolds equation including mass-conserving cavitation by physics informed neural networks (PINNs) with both soft and hard constraints," *Friction*, 2024, doi: 10.1007/s40544-023-0791-1.
[30] Y. Zhao and P. P. L. Wong, "A hybrid data-driven approach for the analysis of hydrodynamic lubrication," *Proceedings of the Institution of Mechanical Engineers, Part J: Journal of Engineering Tribology*, vol. 238, no. 3, pp. 320–331, 2024, doi: 10.1177/13506501231214584.

https://doi.org/10.61319/FZG68FWS